NEUROSCIENCE
RESEARCH ARTICLE
C. Kim, M. J. Chacron / Neuroscience 448 (2020) 43–54

Lower Baseline Variability Gives Rise to Lower Detection Thresholds in Midbrain than Hindbrain Electrosensory Neurons

Chelsea Kim and Maurice J. Chacron *

Department of Physiology, McGill University, Montreal, QC, Canada

Abstract—Understanding how the brain decodes sensory information to give rise to behaviour remains an important problem in systems neuroscience. Across various sensory modalities (e.g. auditory, visual), the time-varying contrast of natural stimuli has been shown to carry behaviourally relevant information. However, it is unclear how such information is actually decoded by the brain to evoke perception and behaviour. Here we investigated how midbrain electrosensory neurons respond to weak contrasts in the electrosensory system of the weakly electric fish *Apteronotus leptorhynchus*. We found that these neurons displayed lower detection thresholds than their afferent hindbrain electrosensory neurons. Further analysis revealed that the lower detection thresholds of midbrain neurons were not due to increased sensitivity to the stimulus. Rather, these were due to the fact that midbrain neurons displayed lower variability in their firing activities in the absence of stimulation, which is due to lower firing rates. Our results suggest that midbrain neurons play an active role towards enabling the detection of weak stimulus contrasts, which in turn leads to perception and behavioral responses.

Key words: Weakly electric fish, envelope, sensory processing, feedback, nonlinear.

INTRODUCTION

Understanding how sensory input is processed by the brain to give rise to behavior remains a central problem in neuroscience. Such understanding is complicated by the fact that natural sensory stimuli display complex spatiotemporal characteristics that frequently consist of a fast time-varying waveform whose amplitude (i.e., the "envelope" or contrast) varies more slowly (Attias and Schreiner, 1997; Joris et al., 2004; Stamper et al., 2013; Theunissen and Elie, 2014). Because such envelopes, which are critical for perception (Shannon et al., 1995, 1998), vary at different frequencies than the underlying carrier, their extraction (i.e., signal demodulation) requires a nonlinear transformation (Rosenberg and Issa, 2011; Stamper et al., 2013; Metzen and Chacron, 2015). Moreover, understanding the neural code is complicated by the fact that descending connections from higher brain areas ('feedback') vastly outnumber ascending connections from the periphery ('feedforward') (Cajal, 1909; Hollander, 1970; Sherman and Guillery, 2002). Previous studies have revealed multiple functions for such feedback pathways such as gain control (Treue and Martinez Trujillo, 1999), enhancing neural responses to particular stimuli (Hupe et al., 1998), or predictive coding (Bastos et al., 2012), with the mechanisms underlying these more or less well understood. More recent studies have shown novel functions for feedback pathways in actually generating neural responses to sensory input but the exact nature of the underlying mechanisms remains unknown (Clarke and Maler, 2017; Metzen et al., 2018).

Gymnotiform wave-type weakly electric fish generate a quasi-sinusoidal electric field surrounding their body through the electric organ discharge (EOD) and sense perturbations of this field through an array of electroreceptor afferents (EAs) located on the skin surface (Turner et al., 1999). These EAs project to pyramidal cells within the hindbrain electrosensory lateral line lobe (ELL), which in turn project to the midbrain torus semicircularis (TS). TS neurons project to higher brain centers to mediate behavioral responses but also massively project back to ELL pyramidal cells, thereby forming a closed-loop (Clarke and Maler, 2017; Metzen et al., 2018) (see (Hofmann and Chacron, 2019) for review). When two conspecifics are located in close proximity to one another, interference between their EODs gives rise to a sinusoidal amplitude modulation (i.e., a beat or first-order) whose frequency is given by the difference between the two EOD frequencies and whose

*Corresponding author. Address: Department of Physiology, McGill University, 3655 Sir William Osler, room 1137, Montreal, QC H3G1Y6, Canada.
E-mail address: maurice.chacron@mcgill.ca (M. J. Chacron).
Abbreviations: AM, amplitude modulation; EA, electroreceptor afferent; ELL, electrosensory lateral line lobe; EOD, electric organ discharge; nP, nucleus praeeminentialis; SIU, stimulus isolation unit; TS, torus semicircularis.

https://doi.org/10.1016/j.neuroscience.2020.09.011
0306-4522/

amplitude (i.e., envelope or second-order) is inversely proportional to the distance between both animals (Yu et al., 2012). The tuning properties of electrosensory neurons that respond to both first- and second-order stimulus attributes have been extensively studied and reviewed (Chacron et al., 2003b, 2011; Marsat et al., 2012; Krahe and Maler, 2014; Clarke et al., 2015; Huang and Chacron, 2017; Metzen and Chacron, 2019). Recent studies have started uncovering the mechanisms that enable electrosensory neurons to respond to second-order attributes (Metzen and Chacron, 2015, 2019; Huang and Chacron, 2016; Huang et al., 2016, 2018, 2019; Metzen et al., 2018). In general, EAs tend to respond to second-order attributes through changes in firing rate when the stimulus intensity (i.e., ~40% contrast) is sufficiently high such as to elicit response nonlinearities such as rectification or saturation (Metzen and Chacron, 2015; Metzen et al., 2018). ELL pyramidal cells instead respond to second-order attributes through increases in firing rate at much lower stimulus intensities (i.e., ~8% contrast), thereby mediating behavioral responses (Metzen et al., 2018). However, such responses are not caused by nonlinear integration of feedforward input from EAs. Rather, they are due to feedback input from midbrain. This is because pharmacological inactivation of closed-loop feedback pathways abolished increases in ELL pyramidal cell firing rate to second-order attributes with weak contrasts as well as the animal's behavioral responses (see (Hofmann and Chacron, 2019) for review). In general, the responses of TS neurons to second-order attributes have been investigated to a much lesser extent. Critically, how TS neurons respond to weak contrasts, to in turn elicit responses from ELL pyramidal cells via feedback, has not been investigated to date.

EXPERIMENTAL PROCEDURES

Animals

This study was conducted using the weakly electric fish *Apteronotus leptorhynchus*. Adult specimens of either sex were purchased from tropical fish suppliers and housed in groups of 2 to 10 in tanks whose water temperature and conductivities were controlled according to published guidelines (26–29 °C, 300–800 μS/cm) (Hitschfeld et al., 2009). Experiments were performed on $N = 52$ fish. All procedures were approved by McGill University's Animal Care Committee under protocol 5285.

Surgery

Surgical procedures were similar to those used in previous studies (Khosravi-Hashemi et al., 2011; Aumentado-Armstrong et al., 2015; Metzen et al., 2016, 2018). For each experiment, an animal was injected intramuscularly with 0.1–0.5 mg of tubocurarine chloride hydrate (Sigma-Aldrich, St-Louis, MO, USA). The animal was then quickly transferred to a tank (30 cm × 30 cm × 10 cm) containing water from the animal's home tank and respirated with heated, oxygenated water passed through its mouth at consistent flow rate of ~10 mL/min. Lidocaine (5%; AstraZeneca, Mississauga, ON, Canada) was then applied to the head region locally and a small craniotomy was performed over the contralateral side. This is because the majority of ELL projections to the contralateral TS come from the ipsilateral ELL (Carr et al., 1981). For ELL recordings, the craniotomy was performed over the ipsilateral side.

Recording

Extracellular recordings from midbrain and hindbrain neurons were achieved with metal-filled micropipettes (Frank and Becker, 1964), as done previously (Chacron et al., 2009; Chacron and Fortune, 2010; Metzen et al., 2018). For midbrain, electrodes were advanced at least 400 μm and up to 1000 μm at approximately coronal section 13 of the published brain atlas in order to target neurons located above layer 6 (Maler et al., 1991). For hindbrain, we used similar techniques to those used previously to target ELL pyramidal cells within the lateral segment (LS). We chose this segment because previous studies have shown that LS neurons displayed overall the greatest sensitivities to sinusoidal envelopes (Huang and Chacron, 2016). There exists two classes of ELL pyramidal cells, namely On- and Off-type that respond with excitation and inhibition to increases in EOD amplitude, respectively (Saunders and Bastian, 1984). Data from ELL On- and Off-type cells were pooled because previous studies have shown that their responses to envelope stimuli, including the one used here, are not significantly different from one another (Huang and Chacron, 2016; Huang et al., 2016, 2019; Metzen et al., 2018). Recordings were obtained from $n = 45$ TS and $n = 196$ ELL neurons. Baseline firing rates (i.e., mean firing rates in the absence of stimulation) were 15.1 ± 8.4 spk/s and 6.9 ± 8.7 spk/s for ELL and TS neurons, respectively. The recorded signals were sampled at 10 kHz and digitized using a Power 1401 with Spike2 software (Cambridge Electronic Design, Cambridge, UK) for offline analysis.

Stimulation

Each animal was presented with stimuli consisting of amplitude modulations (AMs) of its own EOD as done previously (Huang and Chacron, 2016; Huang et al., 2016; Metzen et al., 2018). To generate such stimuli, the animal's EOD zero-crossing points were used to trigger a sinewave generator. At each of these points, the function generator produced one cycle of sinewave at a frequency ~30 Hz greater than EOD frequency, ensuring that this sinewave was synchronized to the animal's EOD. This signal was then multiplied by the stimulus waveform (MT3 multiplier; Tucker Davis Technologies, Alachua, FL, USA), isolated from ground (A395 linear stimulus isolator; World Precision Instruments, Sarasota, FL, USA), and then delivered through a pair of chloridized silver wire electrodes placed 15 cm away from the fish's body on either side. Stimuli consisted of a sinusoidal 5 Hz waveform whose amplitude (i.e., contrast) increases linearly with time between 0 and 100% (Metzen et al., 2018) in order to investigate detection thresholds as well as

band-pass filtered white noise (5–15 Hz, 4th order Butterworth) whose amplitude was sinusoidally modulated at frequencies 0.05, 0.1, 0.2, 0.5, 0.75, and 1.0 Hz that were previously used to investigate neural tuning characteristics (Huang and Chacron, 2016; Huang et al., 2016, 2018). It is important to note that previous studies have shown that similar detection thresholds were found using either 5 Hz sinewaves or 5–15 Hz noise stimuli whose amplitude increases linearly with time (Metzen et al., 2018). Because not all neurons could be held throughout the full length of the stimulation protocol, it was necessary to gather additional data from ELL neurons in response to sinusoidal envelopes. Thus, the number of neurons used for statistical comparison is not the same throughout the manuscript.

Data analysis

All data analysis was performed using MATLAB (MathWorks, Natick, MA, USA). Neural signals were thresholded in order to obtain the spike times. From these, a "binary" sequence with timestep 0.5 ms was constructed by binning time and setting the content of a given bin to 2000 if a spike occurred within it, and to zero otherwise. Note that, as the timestep is less than the absolute refractory period of electrosensory neurons (1–2 ms or higher), there can be at most one spike occurring during any given bin. The resulting sequence was then low-pass filtered (cutoff frequency 0.05 Hz, 2nd order Butterworth filter) to give the time-average firing rate as done previously (Metzen et al., 2018). It is important to note that Metzen et al. (2018) showed that both neural and behavioral detection threshold values were similar for a wide range of filter settings (see their Fig. S1). To assess whether the neural responses were significant, we computed the probability distribution of firing rate values under baseline conditions (i.e., in the absence of stimulation but in the presence of the animal's EOD). Firing rate values comprising the low and high extremities of the probability distribution with less than 0.05 cumulative probability of occurrence were deemed to be significant. The firing rate detection threshold is the lowest value of contrast for which the corresponding firing rate is significantly greater than baseline.

We computed the time-varying vector strength (VS) from the spike times in order to measure the degree of phase-locking to the sinusoidal AM stimulus. Vector strength was computed for each cycle of stimulation:

$$VS = \sqrt{\left(\frac{1}{N}\sum_{i=1}^{N} cos\theta_i\right)^2 + \left(\frac{1}{N}\sum_{i=1}^{N} sin\theta_i\right)^2}. \quad (1)$$

θ_i is the phase of i^{th} spike duration stimulation and N is the total number of spikes. θ_i is obtained from the i^{th} spike time by subtracting the nearest time in the past at which the stimulus is maximum, dividing by the stimulus period, and multiplying by 2π. The time-varying vector strength was obtained by averaging vector strength values over a time window of 1 s. Rayleigh statistics was used to determine the 95% significance level ($VS^2N > 3.5$) as done previously (Metzen et al., 2018). The vector strength detection threshold is the lowest stimulus contrast for which the corresponding vector strength is significant at the 95% level.

As both TS (this study) and ELL (Huang and Chacron, 2016; Huang et al., 2016, 2018) neural populations responded to sinusoidal contrast modulations by sinusoidal modulations in firing rate, we used linear systems identification techniques to characterize the transfer function relating the input to the output. The neural gain (i.e., the amplitude of the transfer function) was computed for each frequency as:

$$Gain = \frac{A_{response}}{A_{stim}}. \quad (2)$$

Here $A_{response}$ is the amplitude (i.e., the difference between the maximum and minimum values of fitted sinewaves to the stimulus cycle-averaged firing rate modulation), while A_{stim} is that of the sinusoidal envelope stimulus. We note that we did not include parts of the stimulus cycle during which the neuron displayed rectification (i.e., cessation of firing) for the fit. We also measured the phase of the transfer function for each frequency as the time relative to stimulus cycle that one must shift the stimulus by such that its maximum occurs at the same time as that of the firing rate response.

RESULTS

The aim of this study was to investigate how TS neurons, which project to higher brain areas to mediate behavior, as well as provide feedback input to ELL pyramidal cells, respond to weak contrast stimuli. As mentioned above, previous experimental results have shown that closed-loop feedback that includes input from TS neurons is necessary to generate an increase in the firing rates of ELL, which is in turn necessary to generate behavioral responses (Metzen et al., 2018) (Fig. 1A). Specifically, in response to a sinusoidal stimulus whose amplitude (i.e., contrast) increases linearly with time (Fig. 1B, top left panel), EAs respond through phase-locking (i.e., action potentials occur preferentially near local maxima of the sinusoidal stimulus) but display no change in firing rate when the contrast is weak enough (Fig. 1A, left). This phase-locking information is sent to ELL pyramidal cells (Fig. 1A, green) which respond to increased contrast with both phase-locking and increases in firing rate (Fig. 1A, pink and blue arrows) and send this information to TS neurons (Fig. 1A, orange). TS neurons project to higher brain areas to mediate behavior (Fig. 1A, right) as well as project back to ELL pyramidal cells via the nP (Fig. 1A, purple). While this closed-loop feedback is necessary in order to generate increases in ELL firing rate to weak contrasts as well as behavioral responses, the underlying mechanisms have not been investigated to date (Fig. 1A, "?"). In this study, we performed electrophysiological recordings from TS neurons in awake behaving animals (Fig. 1B) in order to investigate responses to the same stimuli used previously for EAs and ELL pyramidal cells.

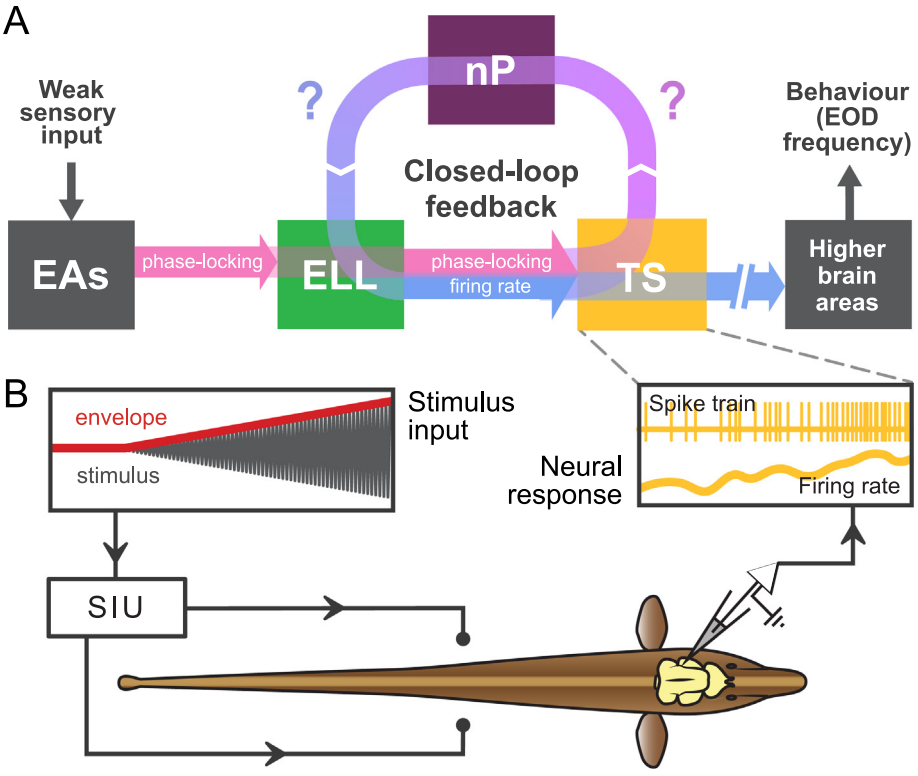

Fig. 1. Electrosensory pathways in *A. leptorhynchus* and experimental setup. **(A)** Weak electrosensory stimuli are first transduced by electroreceptor afferents (EAs, left dark grey) that phase-lock to the sinusoidal first-order stimulus and whose degree of phase-locking increases with stimulus contrast (pink arrow). These project onto ELL pyramidal cells (green). These also phase-lock to the sinusoidal carrier but increase their firing rates in response to increased contrast (blue arrow). ELL pyramidal cells thus send information through both phase-locking and firing rate to the TS (orange), which sends descending projections back to the ELL through the nP via stellate cells (purple). Previous experiments have shown that this closed-loop feedback pathway is necessary to generate increases in ELL pyramidal cell firing rate but does not affect phase-locking and that such increases in firing rate are necessary in order to generate behavioral responses as measured by changes in EOD frequency ((Metzen et al., 2018); right dark grey). **(B)** Experimental setup in which the animal is stimulated via a stimulation isolation unit (SIU), which isolates the stimulus from ground, while neural responses are recorded from TS. (For interpretation of the references to colour in this figure legend, the reader is referred to the web version of this article.)

ELL pyramidal cells respond to weak contrasts through increases in firing rate

To establish a reference to which we can compare the results obtained from TS, we first reproduce a previously published experimental result (Metzen et al., 2018) from a representative example ELL pyramidal cell (Fig. 2). With increasing amplitude (red) of the sinusoidal carrier (grey), this ELL pyramidal cell displayed increased phase-locking as well as increased firing for each carrier cycle (Fig. 2A, insets). Phase-locking was quantified using the vector strength (see Experimental procedures, Fig. 2B), while increases in spiking activity were quantified using the time-averaged firing rate which was obtained by low-pass filtering the spiking activity in order to remove fluctuations during the sinusoidal carrier cycle (see Experimental procedures, Fig. 2C). For both measures, a confidence interval was computed from fluctuations in the absence of stimulation (see Experimental procedures). The stimulus contrast at which either measure crossed the upper bound of the confidence interval was then defined to be the detection threshold (Metzen et al., 2018). It is seen that the firing rate detection threshold was lower than the vector strength detection threshold for this neuron (compare Fig. 2B, C). As mentioned above, previous results have shown that, after feedback inactivation, both the firing rate detection threshold of ELL neurons as well as that of behavior dramatically increases (Metzen et al., 2018). As such, feedback is necessary in order to generate increases in ELL pyramidal cell firing rate to weak contrasts, which are in turn necessary to generate perception and behavior. We further note that we did not see a significant correlation between the firing rate detection threshold and the baseline firing rate ($R = 0.07$, $p = 0.64$, $n = 49$), which strongly suggests that the detection threshold does not depend on ELL pyramidal cell heterogeneities. This is because previous studies have established a strong correlation between the baseline firing rate and heterogeneities within the pyramidal cell population (Bastian and Nguyenkim, 2001; Bastian et al., 2004) (see (Maler, 2009) for review).

Midbrain electrosensory neurons display lower detection threshold values than their hindbrain afferent neurons

We next investigated how TS neurons responded to sinusoidal carriers whose amplitude increases linearly with time. Fig. 3A shows the response of a representative TS neuron (bottom panel) to the stimulus (middle panel). As seen in the insets a and b of Fig. 3A, this neuron tended to phase-lock to the sinusoidal stimulus and, as stimulus contrast increased, the spikes increased in number and occurred more reliably during a subset of phases during the cycle. We quantified TS neural responses by computing both the time-varying vector strength (VS) and time-varying firing rate (FR) (see Experimental procedures) as done previously with the ELL neural responses (see Fig. 2; (Metzen et al., 2018)). Plotting the time-dependent VS (Fig. 3B, top) and FR (Fig. 3C) revealed increases in both quantities with increasing stimulus amplitude. Interestingly, the time-dependent FR increased almost immediately after stimulus onset, which gave rise to a very low FR detection threshold (0.11%; Fig. 3A, blue cross) that is lower than that typically observed for ELL neurons. In contrast, increases in VS

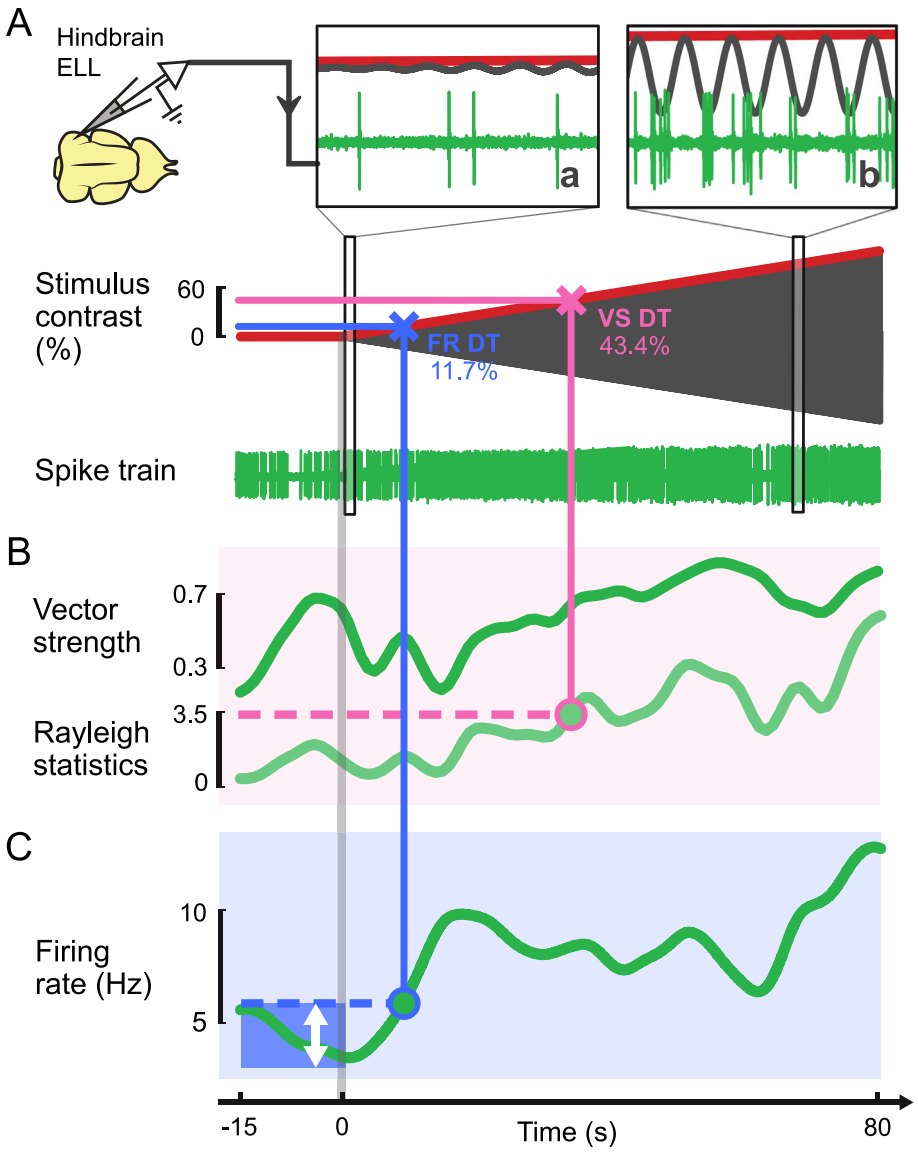

Fig. 2. ELL neurons respond to ramp stimuli. **(A)** A sample extracellular recording from a representative hindbrain ELL neuron responding to a ramp stimulus. Insets a and b demonstrate the changes in spiking activities of this neuron in response to increased stimulus contrast. Notably, with increased contrast the neuron spikes more frequently and at a more consistent phase. **(B)** Time-varying vector strength and Rayleigh statistics for this example ELL neuron. At the point where the value of Rayleigh statistics rises above 3.5 (pink circle), the corresponding stimulus contrast is set to be equal to vector strength detection threshold (panel **A**, pink cross), which was 43.4% for this neuron, which corresponds to 0.58 mV/cm. **(C)** Time-varying firing rate of the same ELL neuron. Firing rate detection threshold is determined based on the interval (white arrow) containing 95% of the probability distribution of baseline firing rate values (blue shaded region). Once the upper limit of this interval is crossed after stimulus onset (blue circle), the corresponding stimulus contrast is taken to be firing rate detection threshold (panel **A**, blue cross), which was 11.7% for this neuron, which corresponds to 0.16 mV/cm. (For interpretation of the references to colour in this figure legend, the reader is referred to the web version of this article.)

were more nuanced, leading to a greater value for detection threshold (2.38%; Fig. 3A, pink cross). Across our TS dataset, we found that detection threshold values obtained from vector strength were similar to those of ELL neurons (Fig. 3D, left panel; p = 0.20, TS: n = 40, ELL: n = 49, Wilcoxon ranksum test). However, detection threshold values obtained from firing rate were significantly lower than those of ELL neurons (Fig. 3D, right panel; p = 3.1e-11, TS: n = 40, ELL: n = 49, Wilcoxon ranksum test).

Lower detection thresholds in TS neurons are due to decreased variability in the absence of stimulation

Why do TS neurons display lower firing rate detection thresholds than ELL pyramidal cells? One possibility is that TS neurons, while having similar baseline variabilities as ELL neurons in the absence of stimulation thereby leading to similar confidence intervals, are more sensitive to increases in the stimulus contrast (i.e., have greater gain). If this hypothesis is correct, then the firing rate of TS neurons should increase more steeply as a function of increasing contrast, such as to cross the upper interval border at a lower contrast (Fig. 4A). To test this hypothesis, we recorded TS neural responses (Fig. 4B, middle orange) to sinusoidal modulations in contrast at different frequencies (Fig. 4B, top), which are independent of the ramps used previously, and measured their sensitivities to these. Importantly, we also recorded ELL neural responses to the same sinusoidal contrast modulations to provide a direct comparison between both neural populations (Fig. 4B, middle green). We found that both neural populations responded through sinusoidal modulations in firing rate (Fig. 4B, bottom) and, as such, used linear systems identification techniques to measure sensitivity (see Experimental procedures). Overall, while the sensitivities of TS neurons were higher than that of ELL neurons (Fig. 4C), the difference between the two was only significant for the highest frequencies, which are not representative of the frequency content of the slowly varying ramps used to compute detection thresholds. Interestingly, sensitivity for TS and ELL neurons both increased as power laws with increasing temporal frequency characterized by similar exponents (Fig. 4D; p = 0.18, TS: n = 16, ELL: n = 62, Wilcoxon ranksum test). As such, our results suggest that the lower firing rate detection thresholds observed for TS neurons, as

compared to ELL pyramidal cells, are not due to differences in sensitivity between both neural populations.

An alternative hypothesis is that TS neurons display lower baseline variability then ELL neurons. This would then lead to a smaller confidence interval overall and thus an earlier crossing point, which would translate to a lower detection threshold as illustrated in Fig. 5A. To test this hypothesis, we measured the baseline variability as the width of the confidence interval of baseline firing activity in TS neurons and compared it to that of ELL neurons (Fig. 5B, white arrows). Overall, the distribution of variability for TS neurons was significantly different than that of ELL neurons (Fig. 5C; p = 3.3e-05, TS: n = 43, ELL: n = 48, two-sample Kolmogorov-Smirnov test), which confirms our hypothesis that differences in detection thresholds are due to differences in variability. Further analysis revealed that the overall baseline mean firing rate of TS neurons was significantly lower than that of ELL neurons (Fig. 5D; p = 3.7e-06, TS: n = 43, ELL: n = 48, two-sample Kolmogorov-Smirnov test); this explains the lower variability, as firing rate ultimately cannot fall below 0 Hz. Further, there was a significant positive correlation between the baseline firing rate and the detection threshold for TS neurons (R = 0.52, p = 0.0004, n = 43). Overall, these results suggest that TS neurons achieve a lower firing rate detection threshold through a lower mean baseline firing rate than ELL, which in turn lowers the variability and facilitates detection of an increase in firing rate.

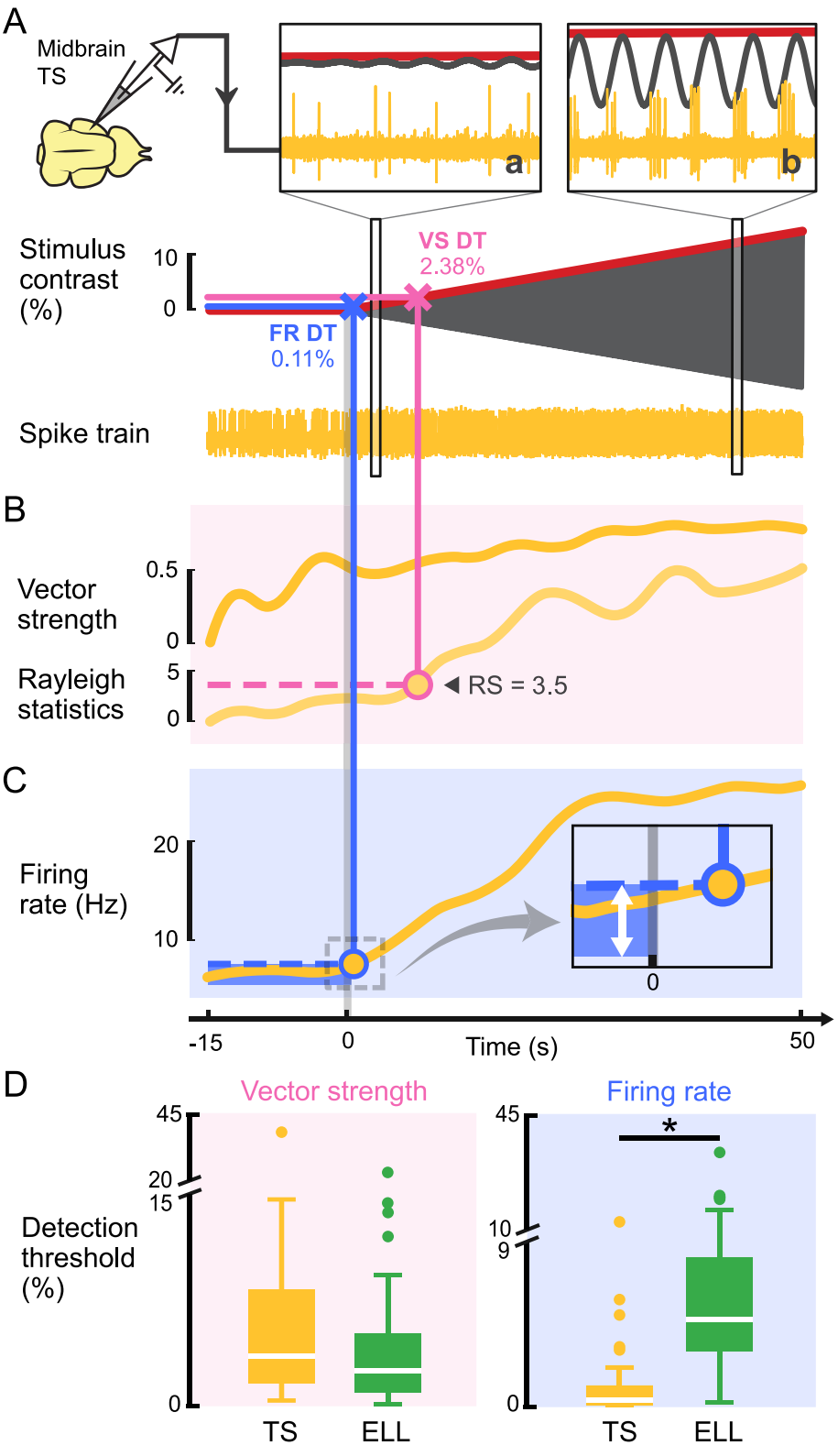

Comparison of detection thresholds observed for TS neurons as well as in other brain areas to behavior

Our results have so far shown that TS neurons display lower detection thresholds of firing rate but are similar in that of vector strength compared to ELL neurons. To better put this into context, we next compare the detection thresholds of ELL, TS, nP stellate cells, and behavior (data from (Metzen et al., 2018)). Fig. 6A shows that, on average, TS neurons displayed lower firing rate detection thresholds than either of ELL, nP stellate cells, or behavior (one-way ANOVA with Bonferroni correction on log-transformed quantities, df = 3, F = 47.39). Fig. 6B shows that, on average, TS neurons displayed lower firing rate detection thresholds than either of ELL, nP stellate cells, or behavior (one-way ANOVA with Bonferroni correction on log-

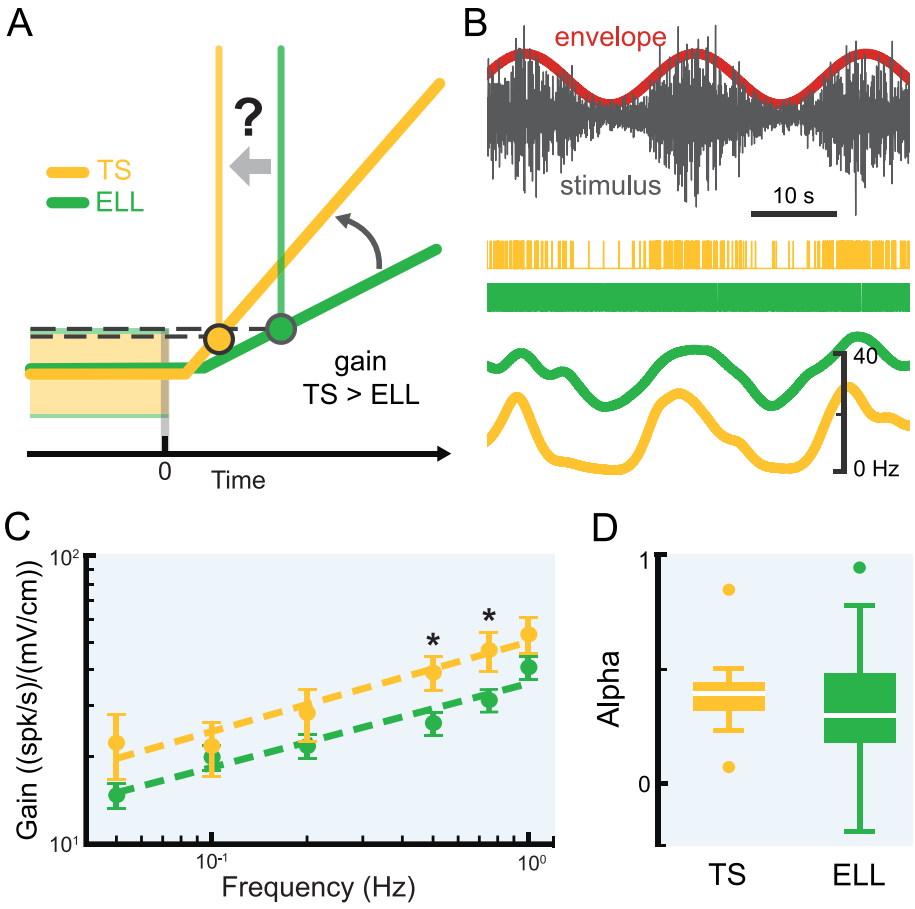

Fig. 4. TS and ELL neurons display similar sensitivity to contrast. **(A)** Illustration showing that, assuming similar baseline firing rate variability for TS and ELL neurons, lower detection thresholds could be achieved if the sensitivity (i.e., "gain" or the slope of the firing rate increase after stimulus onset) of TS neurons (orange) was higher than that of ELL neurons (green). **(B)** Top: A noisy carrier (grey) was modulated sinusoidally (red). Middle: example spiking responses of TS (orange) and ELL (green) neurons to this stimulus. Bottom: Time-dependent firing rates of these same ELL (green) and TS (orange) neurons. **(C)** Population-averaged gain values as a function of frequency for TS (orange) and ELL (green) neurons. No significant difference was observed for the lower frequencies (p = 0.28, 0.78, 0.34, 0.02, 0.03, 0.10 for envelope frequencies 0.05, 0.1, 0.2, 0.5, 0.75, 1.0 Hz, respectively; TS: n = 15–16 and ELL: n = 53–65, Wilcoxon ranksum tests). **(D)** Population-averaged best-fit power law exponent alpha values were not significantly different between TS and ELL (p = 0.18; TS: n = 16 and ELL: n = 62, Wilcoxon ranksum test). (For interpretation of the references to colour in this figure legend, the reader is referred to the web version of this article.)

transformed quantities, df = 3, F = 47.39). This result is surprising given that TS neurons provide the necessary input to generate both the feedback onto ELL pyramidal cells as well as to generate behavioral responses. As further discussed below, we hypothesize that the relatively lower firing rate detection thresholds of TS neurons are due to convergent input from ELL (Fig. 6C). In contrast, because nP stellate cells that project unto ELL pyramidal cells display higher firing rate thresholds than TS neurons on average (Fig. 6B), we hypothesize that there is very little convergence from TS to nP (Fig. 6C). Moreover, anatomical studies suggest that there is little convergence from nP stellate cells onto ELL pyramidal cells as the feedback pathway is topographic (Berman and Maler, 1999). We note that further studies are needed to fully validate these predictions, hence the "?" in Fig. 6C.

DISCUSSION

Summary of results

In this study, we performed electrophysiological recordings from TS neurons in awake behaving animals in order to investigate their responses to contrast increased linearly with time as well as the nature of the underlying mechanisms. Our results show that TS neurons responded to such stimuli through increased phase-locking as well as increased firing rate. Interestingly, increases in firing rate occurred on average for lower contrasts than for ELL neurons (i.e., TS neurons displayed lower firing rate detection thresholds), while there were no significant differences in terms of phase-locking between both neural populations. Further investigation revealed that the

Fig. 3. TS neurons display lower firing rate detection thresholds than ELL neurons. **(A)** A sample extracellular recording from a representative midbrain TS neuron responding to a ramp stimulus. Insets a and b demonstrate the changes in spiking activities of this neuron in response to increased stimulus contrast. Notably, with increased contrast the neuron spikes more frequently and at a more consistent phase. **(B)** Time-varying vector strength and Rayleigh statistics for this example TS neuron. At the point where the value of Rayleigh statistics rises above 3.5 (pink circle), the corresponding stimulus contrast is set to be equal to vector strength detection threshold. In this example, the value is 2.38% (panel **A**, pink cross), which corresponds to 0.012 mV/cm. **(C)** Time-varying firing rate of the same TS neuron. Inset: the firing rate detection threshold is determined based on the interval (white arrow in inset) containing 95% of the probability distribution of baseline firing rate values (blue shaded region). Once the upper limit of this interval is crossed after stimulus onset (blue circle), the corresponding stimulus contrast is taken to be firing rate detection threshold, which is 0.11% for this neuron (panel **A**, blue cross) and corresponds to 0.0005 mV/cm. **(D)** Population-averaged detection threshold values for vector strength (left) and firing rate (right). In each case, TS (left) and ELL (right) are compared. For vector strength, values were not significantly different from one another (p = 0.20; TS: n = 40, ELL: n = 49, Wilcoxon ranksum test). For firing rate, TS neurons displayed significantly lower values than ELL neurons (p = 3.1e-11; TS: n = 40, ELL: n = 49, Wilcoxon ranksum test). (For interpretation of the references to colour in this figure legend, the reader is referred to the web version of this article.)

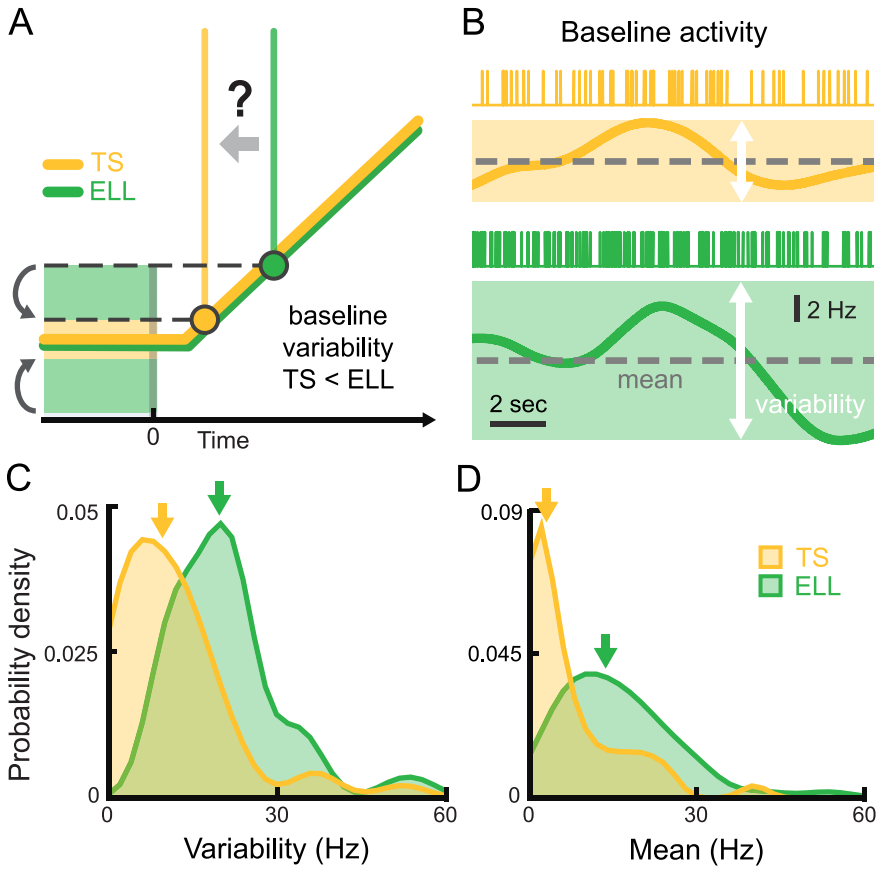

Fig. 5. TS neurons display lower baseline variability than ELL neurons. **(A)** Illustration showing that, if TS and ELL display similar sensitivities, then a lower baseline variability for TS (orange band) would lead to a lower firing rate detection threshold (orange circle) than for ELL (green band and circle). **(B)** Example baseline activity from example TS (top) and ELL (bottom) neurons. Both the mean firing rate (grey dashed line in each panel) and the width of the confidence interval (white arrow in each panel) were computed. **(C)** Distributions of variability (i.e., the width of the confidence interval shown as a white arrow in panel **B**) for TS (orange) and ELL (green) neurons. Both distributions were significantly different from one another (p = 3.3e-05; TS: n = 43, ELL: n = 48, two-sample Kolmogorov-Smirnov test for probability distributions). Arrows indicate median values for each distribution. **(D)** Distributions of mean baseline firing rate (i.e., the mean firing rate in the absence of stimulation shown as dashed grey lines in panel **B**) for TS (orange) and ELL (green) neurons. Both distributions were significantly different from one another (p = 3.7e-06; TS: n = 43, ELL: n = 48, two-sample Kolmogorov-Smirnov test for probability density distributions). Arrows indicate median values for each distribution. We note that the probability density for ELL was lower than that for TS for low (< 7.5 Hz) values of baseline FR variability and mean baseline FR. This simply reflects the fact that, on average, TS neurons tend to display lower mean baseline firing rates as well as variabilities than ELL neurons. (For interpretation of the references to colour in this figure legend, the reader is referred to the web version of this article.)

lower firing rate detection thresholds of TS neurons were due to lower variability in the absence of stimulation rather than differences in sensitivity. Such lower variability most likely results from lower firing rates in the absence of stimulation overall as well as convergent input from ELL neurons.

Feedback and electrosensory processing

Our results have shown that TS neurons displayed lower detection thresholds than both ELL neurons as well as nP stellate cells providing feedback to ELL neurons. This result has important implications for understanding the role played by these neurons in generating both behavioral responses as well as the feedback input to nP stellate cells as well as to ELL neurons.

What are the mechanisms that mediate lower firing rate detection thresholds in TS neurons as compared to ELL neurons? One possibility is that TS neurons display lower firing rate detection thresholds because they receive convergent input from multiple ELL neurons (Fig. 6C), as proposed for the auditory system (Krishna and Semple, 2000). Indeed, summing the activities of multiple neurons can lead to reduction in variability (Zohary et al., 1994). However, the fact that the baseline activities of ELL pyramidal cells are correlated could either be detrimental or beneficial for reducing variability (Zohary et al., 1994; Hofmann and Chacron, 2017). Specifically, while positive correlations are detrimental, negative correlations are instead beneficial. Previous studies have shown that correlations between the baseline activities of ELL pyramidal cells can either be positive or negative (Chacron and Bastian, 2008; Hofmann and Chacron, 2017, 2018). As such, whether correlations between the baseline activities of ELL pyramidal cells are beneficial or detrimental for reducing variability when pooling such activities will depend a lot on which ELL cells converge onto a given TS neuron. Although anatomical studies are needed in order to better understand how input from ELL neurons converges onto TS neurons, electrophysiological studies strongly suggest that TS neurons receive input from both ON- and OFF-type ELL pyramidal cells (McGillivray et al., 2012), which tend to display negative correlations between their baseline activities on average (Hofmann and Chacron, 2017). Thus, we predict that negative correlations between the baseline activities of ELL pyramidal cells will lead to further reduction in baseline variability, thereby leading to lower detection thresholds in TS neurons. Further studies looking at how ELL pyramidal cell populations respond to weak contrast stimuli such as those used here are needed to test this hypothesis.

While a simple summation of convergent ELL activity is likely to be sufficient to observe reduced variability as

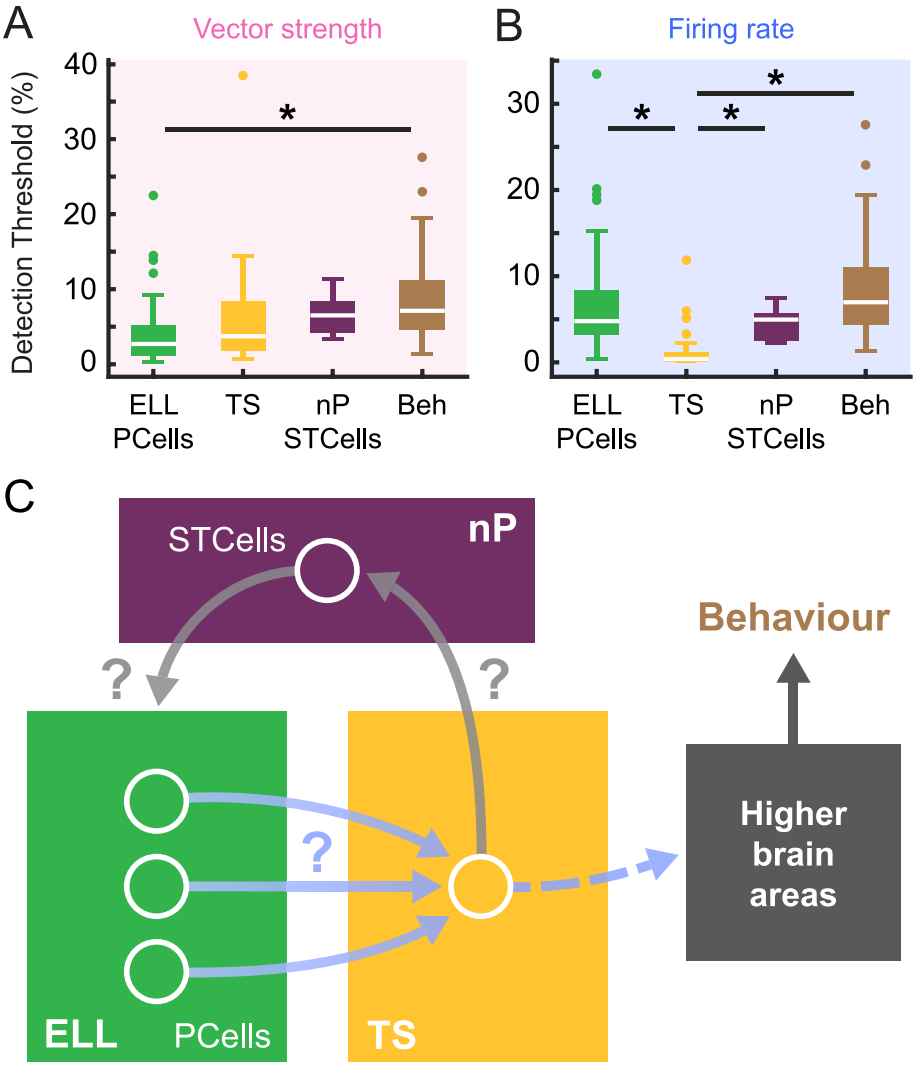

Fig. 6. Comparison of phase locking and firing rate detection thresholds across brain areas and behavior. **(A)** Whisker-box plots showing the vector strength detection thresholds of ELL pyramidal cells, TS, nP stellate cells ("STCells"), and of behavior. All three neuron groups displayed similar detection thresholds, while behavioral detection thresholds were significantly higher than those of ELL neurons (one-way ANOVA with Bonferroni correction on log-transformed quantities, df = 3, $F = 6.14$). **(B)** Whisker-box plots showing the firing rate detection thresholds of ELL, TS, nP stellate cells, and of behavior. TS neurons displayed lower firing rate detection thresholds than either of ELL, nP stellate cells, or behavior (one-way ANOVA with Bonferroni correction on log-transformed quantities, df = 3, $F = 47.39$). **(C)** Putative circuit diagram suggesting that convergence from multiple ELL cells to TS neurons mediate their lower firing rate detection thresholds. The fact that nP stellate cells displayed higher detection thresholds than TS neurons suggests that there is minimal convergence at best. Finally, anatomical studies suggest that there is minimal convergence from nP stellate cells to ELL pyramidal cells as the feedback pathway is topographic (Berman and Maler, 1999).

mentioned above, other mechanisms might further reduce the firing rate detection thresholds of TS neurons. Specifically, previous studies have shown that subthreshold membrane conductances such as T-type calcium channels and voltage-gated sodium channels lead to nonlinear summation of post-synaptic responses (Fortune and Rose, 1997, 2003; Chacron and Fortune, 2010) and therefore shape the temporal filtering properties of TS neurons to current injection (Fortune and Rose, 1997, 2003), as well as help generate directionally selective responses to moving objects (Chacron and Fortune, 2010). However, the degree to which such molecular mechanisms impact the nonlinear integration in TS necessary for increased ELL firing rate response to weak stimuli is unclear. Further studies using intracellular recording techniques should pharmacologically inactivate such conductances in order to test our hypothesis more thoroughly.

Our results have shown that TS neurons with lower baseline firing rates tended to display lower firing rate detection thresholds than their counterparts with higher baseline firing rates. It is likely that TS neurons with lower baseline firing rates correspond to the "sparse" subpopulation, as these neurons are mostly silent except when their preferred stimulus is presented, rather than the "dense" subpopulation which tends to respond to more stimuli and displays higher firing rates overall (Vonderschen and Chacron, 2011; Sproule et al., 2015). While anatomical studies have shown that there are 50 TS neural classes (Carr et al., 1981; Carr and Maler, 1985), the relationship between anatomical and physiological differences is much less clear in TS than in ELL (Sproule et al., 2015), where there is a strong negative correlation between the baseline firing rate and morphology (Bastian and Nguyenkim, 2001; Bastian et al., 2004). In TS, both sparse and dense neurons have been found throughout most if not all layers and TS neurons from most layers project back to nP (Carr et al., 1981; Carr and Maler, 1985; Sproule et al., 2015). As such, it is likely that nP stellate cells receive input from both sparse and dense TS neurons, which might explain why stellate cells display larger firing rate detection thresholds than TS neurons overall (Fig. 6B). It is also conceivable that putative correlations between the activities of TS neurons would hinder any reduction in variability due to convergent input in stellate cells, as discussed above for ELL neurons. Finally, as mentioned above, previous anatomical studies have shown that the direct feedback pathway emanating from stellate cells is highly topographic, with a given stellate cell projecting to at most a few pyramidal

cells (Berman and Maler, 1998, 1999), which could explain why stellate and ELL pyramidal cells display similar firing rate detection thresholds. Further studies are however needed to test all these predictions.

Our results have shown that, while TS neurons displayed lower firing rate detection thresholds than ELL neurons, phase-locking detection thresholds were similar in both neural populations. It is important to note that phase-locking not only carries information about the carrier waveform (e.g., about its frequency content), but also about the contrast. As such, the mechanism observed in the electrosensory system is qualitatively different from those observed previously where feedback can enable the conversion from a temporal code to a rate code (Ahissar et al., 2000). We hypothesize that the information carried through changes in firing rate is more robust to variability, which generally increases in higher order brain areas (Softky and Koch, 1993; Shadlen and Newsome, 1998) and thus ensures accurate perception and behavioral responses. We also note that the variations in contrast considered here contained low (i.e. < 1 Hz) frequencies, and as such do not require information through precise spike timing. It is furthermore important to note that, although our detection threshold measure is largely influenced by baseline (i.e., absence of stimulation) variability, such variability will, in general, determine trial-to-trial variability during stimulation (Risken, 1996; Chacron et al., 2003a, 2005; Mitchell et al., 2018). A reduction in trial-to-trial variability has been shown to be beneficial for neural coding and behavioral performance (Churchland et al., 2010; von Trapp et al., 2016). Further studies are needed to investigate how lower baseline activity and variability in TS neurons shape their trial-to-trial variability during stimulation.

Decoding neural activity to generate perception and behavior

How are changes in ELL neural firing rate in response to weak contrast stimuli decoded downstream in order to give rise to behavior? We note that, because previous results have shown that behavioral detection thresholds were similar to those of single ELL pyramidal cells (Metzen et al., 2018), the timescale at which the organism decides to generate a behavioral response must be much shorter than that at which the amplitude varies for the stimuli used here. Interestingly, our results show that the thresholds of TS neurons are on average lower than behavioral ones. How can single neurons display better performance than the entire organism? Explanations for such a seemingly counterintuitive result have been proposed and involve suboptimal decoding by downstream brain areas due to strong correlations between neural activities (Pitkow et al., 2015). However, whether TS neural activities are correlated at the population level has not been investigated to date and, as mentioned above, should be the focus of future studies. Alternatively, it is possible that behavioral responses are obtained by integrating the activities of ‘‘dense” TS neurons that tend to display higher detection thresholds. Anatomical studies are needed in order to better understand how the activities of TS neurons are combined by downstream brain areas in order to generate behavioral responses.

DATA AVAILABILITY

Data is available from the figshare repository (doi: https://doi.org/10.6084/m9.figshare.9561116).

AUTHOR CONTRIBUTIONS

MJC designed research, CK performed research, CK and MJC wrote the paper.

ACKNOWLEDGEMENTS

We would like to thank C.G. Huang, M.M. Marquez, and M.G. Metzen for gathering the electrophysiological data from ELL neurons.

FUNDING

This research was supported by FRQNT PR 205628 (CK, MJC) and CIHR PJT 159694 (MJC). The funders had no role in study design, data collection and analysis, decision to publish, or preparation of the manuscript.

REFERENCES

Ahissar E, Sosnik R, Haidarliu S (2000) Transformation from temporal to rate coding in a somatosensory thalamocortical pathway. Nature 406:302–306.

Attias H, Schreiner CE (1997) Low-order temporal statistics of natural sounds. Adv Neural Inf Process Systems 9:27–33.

Aumentado-Armstrong T, Metzen MG, Sproule MK, Chacron MJ (2015) Electrosensory midbrain neurons display feature invariant responses to natural communication stimuli. PLoS Comput Biol 11 e1004430.

Bastian J, Nguyenkim J (2001) Dendritic modulation of burst-like firing in sensory neurons. J Neurophysiol 85:10–22.

Bastian J, Chacron MJ, Maler L (2004) Plastic and non-plastic cells perform unique roles in a network capable of adaptive redundancy reduction. Neuron 41:767–779.

Bastos AM, Usrey WM, Adams RA, Mangun GR, Fries P, Friston KJ (2012) Canonical microcircuits for predictive coding. Neuron 76:695–711.

Berman NJ, Maler L (1998) c Distal versus proximal inhibitory shaping of feedback excitation in the electrosensory lateral line lobe: implications for sensory filtering. J Neurophysiol 80:3214–3232.

Berman NJ, Maler L (1999) Neural architecture of the electrosensory lateral line lobe: adaptations for coincidence detection, a sensory searchlight and frequency-dependent adaptive filtering. J Exp Biol 202:1243–1253.

Cajal RS (1909) Histologie du système nerveux de l’Homme et des vertébrés. Paris: Maloine.

Carr CE, Maler L (1985) A Golgi study of the cell types of the dorsal torus semicircularis of the electric fish Eigenmannia: functional and morphological diversity in the midbrain. J Comp Neurol 235:207–240.

Carr CE, Maler L, Heiligenberg W, Sas E (1981) Laminar organization of the afferent and efferent systems of the torus semicircularis of gymnotiform fish: morphological substrates for parallel processing in the electrosensory system. J Comp Neurol 203:649–670.

Chacron MJ, Bastian J (2008) Population coding by electrosensory neurons. J Neurophysiol 99:1825–1835.

Chacron MJ, Fortune ES (2010) Subthreshold membrane conductances enhance directional selectivity in vertebrate sensory neurons. J Neurophysiol 104:449–462.

Chacron MJ, Longtin A, Maler L (2003a) The effects of spontaneous activity, background noise, and the stimulus ensemble on information transfer in neurons. Network: Comput Neural Syst 14:803–824.
Chacron MJ, Longtin A, Maler L (2005) Delayed excitatory and inhibitory feedback shape neural information transmission. Phys Rev E 72 051917.
Chacron MJ, Toporikova N, Fortune ES (2009) Differences in the time course of short-term depression across receptive fields are correlated with directional selectivity in electrosensory neurons. J Neurophysiol 102:3270–3279.
Chacron MJ, Longtin A, Maler L (2011) Efficient computation via sparse coding in electrosensory neural networks. Curr Opin Neurobiol 21:752–760.
Chacron MJ, Doiron B, Maler L, Longtin A, Bastian J (2003b) Non-classical receptive field mediates switch in a sensory neuron's frequency tuning. Nature 423:77–81.
Churchland MM et al (2010) Stimulus onset quenches neural variability: a widespread cortical phenomenon. Nat Neurosci 13:369–378.
Clarke SE, Maler L (2017) Feedback synthesizes neural codes for motion. Curr Biol 27:1356–1361.
Clarke SE, Longtin A, Maler L (2015) Contrast coding in the electrosensory system: parallels with visual computation. Nat Rev Neurosci 16:733–744.
Fortune ES, Rose G (1997) Passive and active membrane properties contribute to the temporal filtering properties of midbrain neurons *in vivo*. J Neurosci 17:3815–3825.
Fortune ES, Rose GJ (2003) Voltage-gated Na + channels enhance the temporal filtering properties of electrosensory neurons in the torus. J Neurophysiol 90:924–929.
Frank K, Becker MC (1964) Microelectrodes for recording and stimulation. In: Physical Techniques in Biological Research (Nastuk WL, ed), pp 23-84. New York: Academic.
Hitschfeld EM, Stamper SA, Vonderschen K, Fortune ES, Chacron MJ (2009) Effects of restraint and immobilization on electrosensory behaviors of weakly electric fish. ILAR J 50:361–372.
Hofmann V, Chacron MJ (2017) Differential receptive field organizations give rise to nearly identical neural correlations across three parallel sensory maps in weakly electric fish. PLoS Comput Biol 13 e1005716.
Hofmann V, Chacron MJ (2018) Population coding and correlated variability in electrosensory pathways. Front Integr Neurosci 12:56.
Hofmann V, Chacron MJ (2019) Novel functions of feedback in electrosensory processing. Front Integr Neurosci 13:52.
Hollander H (1970) The projection from the visual cortex to the lateral geniculate body (LGB). An experimental study with silver impregnation methods in the cat. Exp Brain Res 10:219–235.
Huang CG, Chacron MJ (2016) Optimized parallel coding of second-order stimulus features by heterogeneous neural populations. J Neurosci 36:9859–9872.
Huang CG, Chacron MJ (2017) SK channel subtypes enable parallel optimized coding of behaviorally relevant stimulus attributes: a review. Channels (Austin) 11:281–304.
Huang CG, Zhang ZD, Chacron MJ (2016) Temporal decorrelation by SK channels enables efficient neural coding and perception of natural stimuli. Nat Commun 7:11353.
Huang CG, Metzen MG, Chacron MJ (2018) Feedback optimizes neural coding and perception of natural stimuli. Elife 7 e38935.
Huang CG, Metzen MG, Chacron MJ (2019) Descending pathways mediate adaptive optimized coding of natural stimuli in weakly electric fish. Sci Adv 5(eaax2211).
Hupe JM, James AC, Payne BR, Lomber SG, Girard P, Bullier J (1998) Cortical feedback improves discrimination between figure and background by V1, V2 and V3 neurons. Nature 394:784–787.
Joris PX, Schreiner CE, Rees A (2004) Neural processing of amplitude-modulated sounds. Physiol Rev 84:541–577.
Khosravi-Hashemi N, Fortune ES, Chacron MJ (2011) Coding movement direction by burst firing in electrosensory neurons. J Neurophysiol 106:1954–1968.
Krahe R, Maler L (2014) Neural maps in the electrosensory system of weakly electric fish. Curr Opin Neurobiol 24:13–21.
Krishna BS, Semple MN (2000) Auditory temporal processing: responses to sinusoidally amplitude-modulated tones in the inferior colliculus. J Neurophysiol 84:255–273.
Maler L (2009) Receptive field organization across multiple electrosensory maps. I. Columnar organization and estimation of receptive field size. J Comp Neurol 516:376–393.
Maler L, Sas E, Johnston S, Ellis W (1991) An atlas of the brain of the weakly electric fish *Apteronotus Leptorhynchus*. J Chem Neuroanat 4:1–38.
Marsat G, Longtin A, Maler L (2012) Cellular and circuit properties supporting different sensory coding strategies in electric fish and other systems. Curr Opin Neurobiol 22:686–692.
McGillivray P, Vonderschen K, Fortune ES, Chacron MJ (2012) Parallel coding of first- and second-order stimulus attributes by midbrain electrosensory neurons. J Neurosci 32:5510–5524.
Metzen MG, Chacron MJ (2015) Neural heterogeneities determine response characteristics to second-, but not first-order stimulus features. J Neurosci 35:3124–3138.
Metzen MG, Chacron MJ (2019) Envelope Coding and processing: implications for perception and behavior. In: Carlson B, Sisneros J, Popper A, Fay R, editors. Electroreception: Fundamental Insights from Comparative Approaches. Cham: Springer. p. 251–277.
Metzen MG, Hofmann V, Chacron MJ (2016) Neural correlations enable invariant coding and perception of natural stimuli in weakly electric fish. Elife 5 e12993.
Metzen MG, Huang CG, Chacron MJ (2018) Descending pathways generate perception of and neural responses to weak sensory input. PLoS Biol 16 e2005239.
Mitchell DE, Kwan A, Carriot J, Chacron MJ, Cullen KE (2018) Neuronal variability and tuning are balanced to optimize naturalistic self-motion coding in primate vestibular pathways. Elife 7 e43019.
Pitkow X, Liu S, Angelaki DE, DeAngelis GC, Pouget A (2015) How can single sensory neurons predict behavior? Neuron 87:411–423.
Risken H (1996) The Fokker-Planck equation. Berlin: Springer.
Rosenberg A, Issa NP (2011) Visual demodulation by the Y cell pathway. Neuron 71:348–361.
Saunders J, Bastian J (1984) The physiology and morphology of two classes of electrosensory neurons in the weakly electric fish *Apteronotus Leptorhynchus*. J Comp Physiol A 154:199–209.
Shadlen MN, Newsome WT (1998) The variable discharge of cortical neurons: implications for connectivity, computation, and information coding. J Neurosci 18:3870–3896.
Shannon RV, Zeng FG, Wygonski J (1998) Speech recognition with altered spectral distribution of envelope cues. J Acoust Soc Am 104:2467–2476.
Shannon RV, Zeng FG, Kamath V, Wygonski J, Ekelid M (1995) Speech recognition with primarily temporal cues. Science 270:303–304.
Sherman SM, Guillery RW (2002) The role of the thalamus in the flow of information to the cortex. Philos Trans Royal Soc London - Series B: Biol Sci 357:1695–1708.
Softky WR, Koch C (1993) The highly irregular firing of cortical cells is inconsistent with temporal integration of random EPSPs. J Neurosci 13:334–350.
Sproule MKJ, Metzen MG, Chacron MJ (2015) Parallel sparse and dense information coding streams in the electrosensory midbrain. Neurosci Lett 607:1–6.
Stamper SA, Fortune ES, Chacron MJ (2013) Perception and coding of envelopes in weakly electric fishes. J Exp Biol 216:2393–2402.
Theunissen FE, Elie JE (2014) Neural processing of natural sounds. Nat Rev Neurosci 15:355–366.

Treue S, Martinez Trujillo JC (1999) Feature-based attention influences motion processing gain in macaque visual cortex. Nature 399:575–579.

Turner RW, Maler L, Burrows M (1999) Electroreception and electrocommunication. J Exp Biol 202:1167–1458.

von Trapp G, Buran BN, Sen K, Semple MN, Sanes DH (2016) A decline in response variability improves neural signal detection during auditory task performance. J Neurosci 36:11097–11106.

Vonderschen K, Chacron MJ (2011) Sparse and dense coding of natural stimuli by distinct midbrain neuron subpopulations in weakly electric fish. J Neurophysiol 106:3102–3118.

Yu N, Hupe G, Garfinkle C, Lewis JE, Longtin A (2012) Coding conspecific identity and motion in the electric sense. PLoS Comput Biol 8 e1002564.

Zohary E, Shadlen MN, Newsome WT (1994) Correlated neuronal discharge rate and its implications for psychophysical performance. Nature 370:140–143.

(Received 23 April 2020, Accepted 2 September 2020)
(Available online 11 September 2020)